

Entanglement properties of the antiferromagnetic-singlet transition in the Hubbard model on bilayer square lattices

Chia-Chen Chang, Rajiv R. P. Singh, and Richard T. Scalettar
Department of Physics, University of California Davis, CA 95616, USA

We calculate the bipartite Rényi entanglement entropy of an $L \times L \times 2$ bilayer Hubbard model using a determinantal quantum Monte Carlo method recently proposed by Grover [Phys. Rev. Lett. **111**, 130402 (2013)]. Two types of bipartition are studied: (i) One that divides the lattice into two $L \times L$ planes, and (ii) One that divides the lattice into two equal-size ($L \times L/2 \times 2$) bilayers. We compare our calculations with those for the tight-binding model studied by the correlation matrix method. As expected, the entropy for bipartition (i) scales as L^2 , while the latter scales with L with possible logarithmic corrections. The onset of the antiferromagnet to singlet transition shows up by a saturation of the former to a maximal value and the latter to a small value in the singlet phase. We comment on the large uncertainties in the numerical results with increasing U , which would have to be overcome before the critical behavior and logarithmic corrections can be quantified.

PACS numbers: 03.65.Ud, 71.10.Fd, 75.10.Jm

I. INTRODUCTION

There are several reasons for recent excitement in the condensed matter theory community regarding quantum entanglement entropies of many-body lattice models.^{1,2} These entropies connect widely disparate fields of physics such as quantum information theory, quantum gravity and black holes with the many-body description of quantum phases and material science. When a macroscopic system is divided into two parts, the bipartite entanglement entropies provide universal signatures of quantum phase transitions and critical phenomena¹⁻³ and have also been used to demonstrate existence of topological quantum phases in spin models.⁴⁻⁹

In a typical eigenstate of a many-body Hamiltonian, these entropies are extensive i.e., in a large system they are proportional to the volume of the system and are closely related to the thermal entropy.¹⁰⁻¹² However, in the many-body ground state, such entropies typically obey an “area-law”,¹³ that is they scale with the measure of the “area” or boundary between subsystems. Such an “area-law” provides the basis for novel approaches for quantum many-body systems including density matrix renormalization group (DMRG) and their higher-dimensional tensor-network generalizations.¹⁴⁻¹⁶

Despite this progress, unbiased numerical calculations of entanglement entropies in interacting lattice models of spatial dimensionality greater than one remain a big challenge. Over the last few years several methods have been developed for quantum spin models, which go beyond the very small finite-systems for which exact eigenstates, reduced density matrices and entanglement entropies can be calculated by standard Lanczos type methods. The first such method is the quantum Monte Carlo (QMC) method, which allows unbiased stochastic simulation of large systems.^{17,18} A second method is that of series expansions, where entanglement entropies are obtained as a power-series expansion in a suitable coupling constant.¹⁹⁻²¹ A third method is that of numerical linked

cluster expansion (NLCE), where the entanglement properties of the thermodynamic system are expressed as a sum over the contributions from different sized clusters, which can be evaluated numerically through exact diagonalization.^{22,23}

Different methods have their advantages and disadvantages. The QMC method deals with finite systems and its convergence can be rigorously established by sufficient sampling. One then needs an extrapolation to the thermodynamic limit. Since rather large system sizes can be simulated many quantities can be calculated with high accuracy. The series expansion method is particularly suitable for a system in which a small parameter exists. In that limit, it provides highly accurate answers in the thermodynamic limit. However, critical points necessarily lie at the boundary of the convergence radius of the series, and thus studying critical properties requires the use of series extrapolation methods.²⁴ Both QMC and series expansion methods are suitable for calculating Rényi entropies of low integer order. In contrast the NLCE method, can be used to calculate any index Rényi or von Neumann entanglement entropy. Series expansions and NLCE are also particularly useful for studying entanglement contributions from corners and other subleading manifolds as those contributions can be analytically isolated from those of other larger boundaries.

Unbiased calculations of entanglement properties of interacting lattice fermion systems in dimensionality greater than one, have only recently been initiated. In a system with only bilinear fermion terms in the Hamiltonian, the correlation matrix method provides a very efficient method.²⁵⁻²⁷ This technique is very powerful, allowing for calculations of ground state, excited state, finite-temperature or non-equilibrium entropy. All Rényi or von Neumann entropies can be computed with similar ease. Recently, an unbiased approach for treating interacting fermion systems was proposed by Grover.²⁸ It uses the determinant quantum Monte Carlo (DQMC) method to calculate the low integer Rényi entropies.^{28,29} This is the method we employ here.

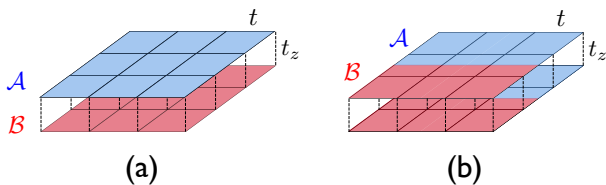


FIG. 1. (Color online) Subsystem partitions studied in this work: (a) single layer, (b) two half-layers. The corresponding entanglement entropies are denoted by S_2^s and S_2^h respectively.

The bilayer Hubbard model is a particularly simple model that is known to have several phase transitions.^{30–32} In the large U limit, it reduces to the bilayer Heisenberg model, which has been extensively studied by quantum Monte Carlo simulations and other methods.^{33–35} When the interlayer coupling is weak the model has a Néel ordered phase. When the interlayer coupling is strong, it has a spin-gapped singlet phase. The two phases are separated by a second phase order transition. It has been shown numerically that the transition is in the universality class of the three-dimensional classical Heisenberg model.³³

The entanglement entropy offers a potentially very interesting way of studying this model. In addition to the possible signature of the phase transition, the entanglement entropy can also provide a measure of the Fermi surface properties of the system. It is well known that in non-interacting fermion systems, there is a logarithmic breakdown of the “area-law”. Furthermore, this breakdown can be related via the Widom conjecture to quantitative geometrical features of the Fermi-surface relative to the boundary partitioning the two subsystems.^{12,36–40} Thus, entanglement entropy can provide a direct evidence for a Fermi surface and hence a metallic phase in the model.

In this work, we study entanglement properties in the antiferromagnet (AF) to band insulator (BI) transition of the bilayer Hubbard model. We study two bipartitions of the lattice, where the lattice is divided into two planes and the other where the system is split up into two halves along one of the axis of the square-lattice, as illustrated in Fig. 1. Our study of the tight-binding model further confirms the Widom conjecture. One can also see the metal to band-insulator transition and associated singularity in the tight-binding model study. For the Hubbard model, entanglement properties are examined as a function of interlayer hopping. We also discuss challenges in extracting critical properties of the Rényi entropy and suggest possible solutions.

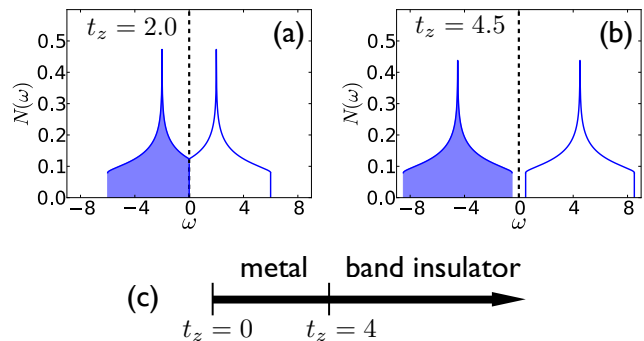


FIG. 2. (Color online) Panel (a) and (b): Non-interacting density of states of the half-filled bilayer system at $t_z = 2.0$ and $t_z = 4.5$ respectively. The Fermi level is at $\omega = 0$. (c): Non-interacting phase diagram of the model Eq. (1).

II. BILAYER SQUARE LATTICE HUBBARD MODEL

The bilayer square lattice Hubbard model is defined by the following Hamiltonian

$$\begin{aligned}
 H = & -t \sum_{\ell\sigma} \sum_{\langle ij \rangle} \left(c_{i\ell\sigma}^\dagger c_{j\ell\sigma} + h.c. \right) \\
 & - t_z \sum_{i\sigma} \left(c_{i1\sigma}^\dagger c_{i2\sigma} + h.c. \right) \\
 & + U \sum_{i\ell} \left(n_{i\ell\uparrow} - \frac{1}{2} \right) \left(n_{i\ell\downarrow} - \frac{1}{2} \right) - \mu \sum_{i\ell\sigma} n_{i\ell\sigma}. \quad (1)
 \end{aligned}$$

Here $c_{i\ell\sigma}^\dagger$ ($c_{i\ell\sigma}$) creates (annihilates) an electron at site \mathbf{i} with spin $\sigma \in \{\uparrow, \downarrow\}$ on an $L \times L \times 2$ lattice. $\ell \in \{1, 2\}$ is the layer index. t and t_z are intra- and inter-layer hoppings respectively. $U > 0$ is the onsite repulsion, and the chemical potential μ determines the density of the system. We measure the energy in units of $t = 1$. The chemical potential is kept at $\mu = 0$ so that the system stays half-filled.

In the tight-binding limit, $U = 0$, the physics of the system is determined solely by the inter-layer hopping t_z . As demonstrated in Fig. 2, at $t_z \leq 4$ the system is in metallic phase with fully nested bonding and anti-bonding Fermi surfaces and finite density of states at the Fermi level. For $t_z > 4$, a gap opens up at the Fermi level and the system becomes a band insulator. The phase transition at $U = 0$ is associated with the closing of the gap in the particle-hole excitation spectra and this gap closes continuously.

At finite U , the model has been studied by several groups using numerical methods such as QMC,^{30,41} dynamical mean-field theory (DMFT)³¹ and variational Monte Carlo (VMC).³² These studies generally agree that at large U , there is a direct transition from a singlet to a Néel phase as the inter-layer hopping is varied. However, properties of the model at small U remain controversial. Is there a direct transition from a singlet to

a Néel phase as inter-layer hopping matrix elements is varied? Both DQMC and DMFT studies suggest a paramagnetic metal phase. However, in roughly the same parameter range, the VMC study predicts a Néel phase. We will not address details of the phase diagram in this paper. Rather, we will examine entanglement properties of the system across the phase transition at small U where there are no exact results.

III. RÉNYI ENTANGLEMENT ENTROPY

For a quantum many-body system divided into two disjoint subsystems \mathcal{A} and \mathcal{B} , one can define a reduced density matrix for subsystem \mathcal{A} by tracing out the degrees of freedom in \mathcal{B} : $\rho_{\mathcal{A}} = \text{Tr}_{\mathcal{B}}(|\Psi\rangle\langle\Psi|)$, where $|\Psi\rangle$ is the ground state of the total system. Then the Rényi entanglement entropy can be calculated from $\rho_{\mathcal{A}}$ as

$$S_n = \frac{1}{1-n} \log [\text{Tr}(\rho_{\mathcal{A}}^n)], \quad (2)$$

where the von Neumann entropy can be recovered in the $n \rightarrow 1$ limit. In this paper, we focus on the second Rényi entanglement entropy, i.e. $n = 2$. For the bilayer square lattice, we consider two different subsystem partitions shown in Fig. 1 and label the corresponding second Rényi entropy as S_2^s and S_2^h respectively.

When there is no interaction, the model can be treated as two independent collections of spinless free fermions. In this case, the reduced density matrix $\rho_{\mathcal{A}}$ factorizes and, for each collection, the second Rényi entropy can be expressed in terms of eigenvalues of the correlation matrix defined as^{25–27}

$$C_{\mathbf{i}\mathbf{j}} = \langle c_{\mathbf{i}}^\dagger c_{\mathbf{j}} \rangle \quad (3)$$

where $\mathbf{i}, \mathbf{j} \in \mathcal{A}$, and $\langle \dots \rangle$ denotes the expectation value with respect to the ground state. We numerically diagonalize the tight-binding Hamiltonian and construct $C_{\mathbf{i}\mathbf{j}}$ using the ground state orbitals. Let λ_k denote the eigenvalues of $C_{\mathbf{i}\mathbf{j}}$, then the Rényi entropy S_2 is given by

$$S_2 = - \sum_k \log [\lambda_k^2 + (1 - \lambda_k)^2]. \quad (4)$$

For interacting itinerant fermions, the correlation matrix method is not applicable and measuring entanglement properties of the system often requires the knowledge of the ground state wave function. Recently, there have been proposals of computing the Rényi entropy for lattice fermions using QMC technique that does not require the access of the ground state wave function. For example, by writing S_2 as a ratio of partition functions, a generic scheme based on path integral Monte Carlo was developed in Ref. 18. This method has been successfully applied to the single-band Hubbard model in one dimension⁴², and becomes the basis of a more recent proposal of computing S_2 within the DQMC scheme.⁴³

In this work, we adopt the scheme proposed in Ref. 28. This technique exploits the fact that DQMC maps interacting fermions into a system of free fermions coupled to fluctuating auxiliary fields. For a given set of auxiliary fields, the trace in Eq. (2) can then be carried out explicitly, and the second Rényi entropy is expressed as²⁸

$$S_2 = - \log \left\{ \sum_{\{s\}, \{s'\}} \mathcal{P}_s \mathcal{P}_{s'} \det \left[G_{\mathcal{A}}(s) G_{\mathcal{A}}(s') + (\mathbf{I} - G_{\mathcal{A}}(s))(\mathbf{I} - G_{\mathcal{A}}(s')) \right] \right\}. \quad (5)$$

Here $\{s\}$ and $\{s'\}$ represent two sets of auxiliary fields. $\mathcal{P}_s, \mathcal{P}_{s'}$ are the probability distribution used to sample the fields. $G_{\mathcal{A}}(s)$, and similarly $G_{\mathcal{A}}(s')$, are one-particle Green's function whose spatial indices are restricted within the subregion \mathcal{A} . \mathbf{I} is the identity matrix. While the technique allows the measurement of higher order Rényi entropies S_n ,^{28,29} it cannot directly access the von Neumann entanglement entropy. Measuring S_n requires n replica of subsystems. As a result, the computation of S_n is significantly more demanding, and not much more informative²². Therefore, in this work we only focus on S_2 .

IV. RESULTS AND DISCUSSIONS

A. Non-interacting bilayer model

We first discuss entanglement properties for free electrons on the bilayer square lattice. Fig. 3 summarizes the second Rényi entropy as a function of t_z . Both S_2^s and S_2^h show a sharp signal at the critical point $t_z = 4.0$. For the first partition where subsystem \mathcal{A} is a single layer (c.f. Fig. 1), S_2^s approaches the value $4(L-1)\ln 2$ when $t_z \rightarrow 0$, which, surprisingly, is different from $t_z = 0$ case, where it vanishes identically. To understand the results, let us recall that for $t_z = 0$, the ground state can be chosen independently in the two planes. There should be no entanglement. However, ground state degeneracy leads to finite entanglement for infinitesimal t_z . To see this, consider the Fermi surfaces with t_z set to zero. In each plane, and for each spin component, the Fermi surface consists of the diamond-shape boundary of the antiferromagnetic Brillouin zone at half-filling. For an $L \times L$ square lattice, exactly $2L - 2$ \mathbf{k} -points lie on the Fermi surface for each spin component. Half of them will be occupied and the other half will be unoccupied. This degeneracy is lifted by an infinitesimal t_z , which leads to equal number of bonding and anti-bonding states with all the bonding states having negative energy and all the anti-bonding states having positive energy. Thus, at non-zero t_z , all the bonding states will be occupied and anti-bonding states empty. Each occupied bonding state contributes $\ln 2$ to the entanglement entropy between the

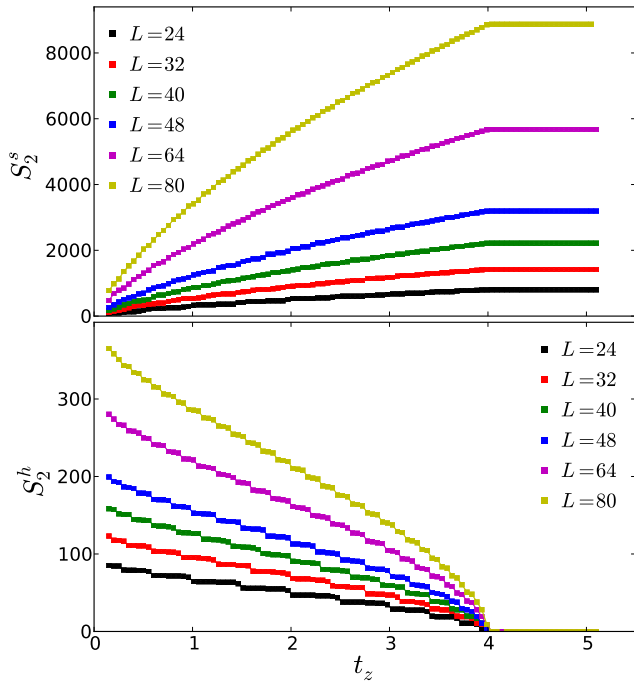


FIG. 3. (Color online) The second Rényi entropy as a function of inter-layer hopping t_z for non-interacting electrons on bilayer square lattices at half-filling. L is the linear dimension of the bilayer lattice. The plateau structure seen in the figures for $t_z < 4$ is caused by the ground state degeneracy at the Fermi surfaces of free electrons on finite lattices.

planes. There are $(2L - 2)$ \mathbf{k} -points where such bonding states happen at the Fermi surface for each spin component. This gives us a total entanglement entropy between the planes of $4(L - 1) \ln 2$.

In the insulating phase $t_z \geq 4.0$, the system consists of localized singlet pairs across the layers. We observe that $S_2^s = 2L^2 \ln 2$. This is because for free electrons, each spin component (up or down) contributes $\ln 2$ to the entropy at each site since the bonding state is occupied. Thus, the total entanglement entropy for the free fermion bilayer is $2L^2 \ln 2$. Alternatively, the free-fermion singlet state on every pair of sites of the bilayer has $\ln 4$ entropy because the reduced density matrix has four equally likely choices: empty, spin-up, spin-down, both present. As a result, the total entropy is also $L^2 \ln 4 = 2L^2 \ln 2$ as there are L^2 pairs of sites.

The second Rényi entropy behaves quite differently for the second partition where \mathcal{A} has two half-layers. In particular, S_2^h decreases monotonically with increasing t_z . In the insulating phase where the lattice is filled with localized singlet pairs, $S_2^h = 0$ since \mathcal{A} and the rest of the lattice are decoupled completely.

Next we move on to examine scaling properties of S_2 . In the band insulator phase, the previously mentioned result $S_2^s = 2L^2 \ln 2$ indicates that S_2^s scales as the “volume” of \mathcal{A} , i.e. L^2 . To examine the scaling behavior of S_2^s in the metallic phase, we plot in the top panel of Fig. 4

S_2^s/L^2 versus the linear dimension L of the subsystem for $t_z < 4.0$. The data are fitted to a linear function and the results are shown as dotted lines in the figure. Within regression uncertainties, the slope of the fit is essentially zero, implying that $S_2^s \sim L^2$. In other words, S_2^s obeys a “volume law”. This result is a consequence of the fact that the interfacial area due to the partition scales as L^2 .

The entanglement properties for the second partition (two half-layers) are more intricate in the range $t_z < 4.0$. Since the orientation of the boundary between \mathcal{A} and \mathcal{B} and the normal vector of the Fermi surfaces are no longer perpendicular, the behavior of S_2^h is closely connected to the local geometry of Fermi surfaces. In the bottom panel of Fig. 4, we show the scaling of S_2^h in the metallic phase. Dotted lines in the figure are fits to the data according to the formula $S_2^h/L = \alpha \ln L + \beta$. Instead of an “area law” where $S_2^h \sim L$, the result of the fits shows that there is a logarithmic correction to the area law. We note that in the bottom panel of Fig. 4, there are outliers in the S_2^h/L versus $\ln L$ plot at $t_z = 1.312$, 2.726 , and 3.736 . These fluctuations result from finite-size effects produced by ground state degeneracy at the Fermi level. Such effects have strong dependence on L and t_z .

For free fermions such a logarithmic correction to the area-law is expected.³⁷ The coefficient of the logarithmic correction has been derived in Ref. 44 based on the Widom conjecture:⁴⁵

$$\alpha(t_z) \sim \int_{\text{FS}} |\hat{n}_{\mathbf{x}} \cdot \hat{n}_{\mathbf{k}}| dS_{\mathbf{x}} dS_{\mathbf{k}}. \quad (6)$$

The integral is carried out over the surfaces of the subsystem and the Fermi surface. $\hat{n}_{\mathbf{x}}$ and $\hat{n}_{\mathbf{k}}$ are the unit normal vectors to the surfaces. In Fig. 5, we compare the exact result of free fermions and the coefficient $\alpha(t_z)$ extracted from the fits. The agreement is reasonably good and supports the Widom conjecture for the bilayer tight-binding model.

B. Bilayer Hubbard model

The behavior of the second Rényi entropy for the bilayer Hubbard model is shown in Fig. 6 at temperature $T/t = 0.05$. We have done simulations at different temperatures and made sure the results are not changing with temperature when T/t reaches 0.05. As indicated by Eq. (5), the method relies on computing the determinant of single particle Green’s functions, which become ill-conditioned at large U/t values⁴⁶. Therefore the interaction strength will be constrained in the range $U/t \leq 4.0$ in our work.

Using Eq. (5), the Monte Carlo procedure accumulates statistics for the trace of the squared reduced density matrix $\text{Tr}(\rho_{\mathcal{A}}^2)$, and the Rényi entropy is a derived quantity from the final results. To obtain a reliable estimation of S_2 and minimize possible bias, we use the jackknife resampling method to estimate S_2 and its statistical error.

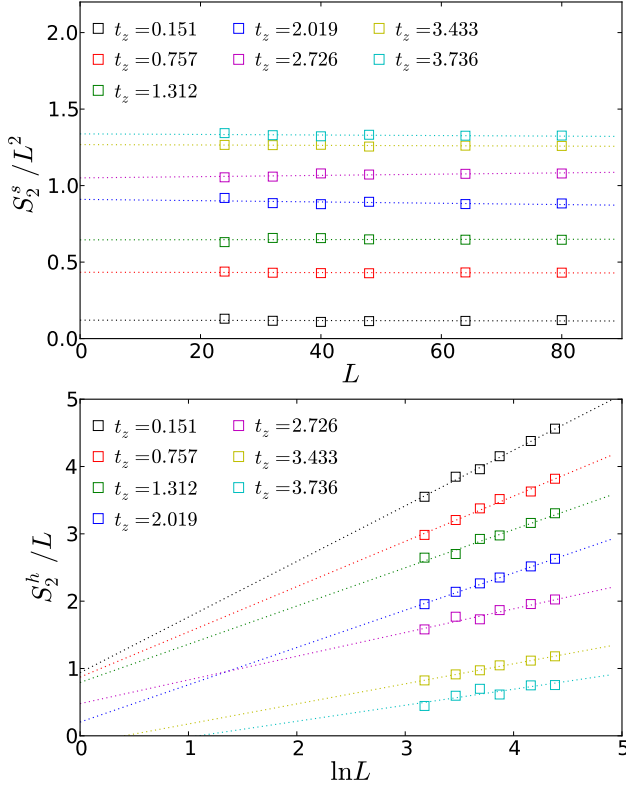


FIG. 4. (Color online) Scaling properties of S_2^s (top) and S_2^h (bottom) for the non-interacting bilayer model. Dotted lines represent linear fits to the data extracted from Fig. 3 at selected t_z 's.

We also average the data over periodic and anti-periodic boundary conditions in order to reduce finite-size effects.

Fig. 6 (a)-(c) summarize S_2 for the single-layer partition at $U = 1.0, 2.0$, and 4.0 . The overall behavior of S_2^s as a function of t_z is similar to that for free fermions: the entanglement entropy increases monotonically with t_z and saturates when $t_z \gtrsim t_z^c$. For comparison, we also plot S_2^s of free fermions for $L = 10$ and 12 . The data (represented by empty diamonds) is consistent with the bilayer Hubbard model results, albeit finite-size fluctuations are much stronger in the free fermion data. At a given L , the maximal value of S_2^s for the bilayer Hubbard model agrees with the free fermion result. This, again, is due to the fact that S_2^s only picks up short-range entanglement between singlet pairs across the two layers. We speculate that the observed critical t_z^c in the bilayer Hubbard model also corresponds to the place where the singlets start to break-up, indicating the onset of the singlet to AF transition. For $U = 1.0$ and 2.0 , $t_z^c \sim 4.0$; while at $U = 4.0$, the entanglement entropy plateaus at a slightly lower $t_z^c \sim 3.5$. Interestingly, these values are very close to the AF-BI transition phase boundary predicted by the VMC study.³²

Next we turn our attention to the two half-layers partition. Simulations are carried out at weak to moderate

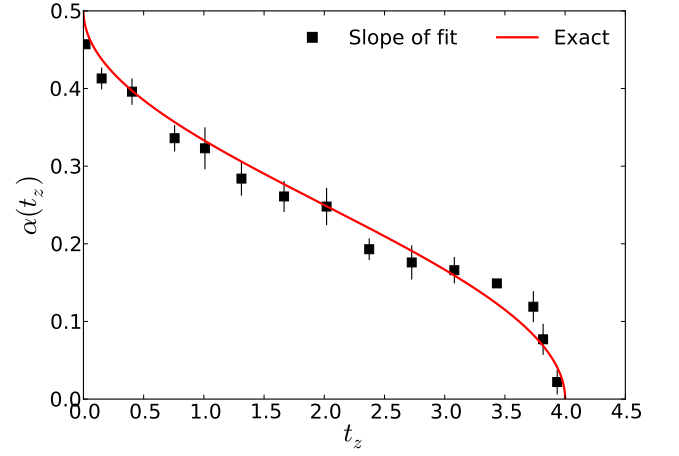


FIG. 5. (Color online) Filled squares represent the coefficient of the fit $S_2^h/L = \alpha \ln L + \beta$ as a function of interlayer hopping t_z . The vertical line denotes the uncertainty of the regression. The solid curve is the function $\alpha(t_z) = 1/(2\pi) \cos^{-1}(t_z/2 - 1)$ derived using Eq. (6) for the non-interacting bilayer model.

coupling strengths. Although details of the phase diagram in this parameter range are still under debate, it is generally agreed that at $U \gtrsim 4$, there is a direct AF to BI transition.³⁰⁻³² In the Heisenberg limit where $U \rightarrow \infty$, however, the phase transition is well characterized.³³⁻³⁵ Recently it has also been shown that the leading area-law coefficient shows a local maximum at the quantum critical point,⁴⁷ signaling the phase transition in the Heisenberg square-lattice bilayer.

The Rényi entropy S_2^h as a function of the inter-layer hopping t_z is plotted in Fig. 6 (d)-(e), at temperature $T/t = 0.05$ and $U = 1.0, 2.0$, and 4.0 respectively. As a reference, the free fermion S_2^h data is also shown in the same figures for $L = 10$ and 12 (empty diamonds). The plateau-like structure in the free-fermion data is caused by the degeneracy at the Fermi surfaces on a finite lattice. At $U = 1$, the S_2^h data still show kinks near the edge of the $U = 0$ plateaus. As the interaction strength is increased, the kinks become less pronounced. This suggests that the $U = 0$ finite-size fluctuations can get carried over at small U s and produce the kinks. A general trend of S_2^h for the system is that it reduces with increasing t_z . However, unlike the free fermion case, here the Rényi entropy converges at a very slow rate to a low value for $t_z \gtrsim 4.0$. The comparison between the free fermion and the Hubbard model data suggests that S_2^h gets enhanced, particularly in the region $t_z \lesssim 3.0$, by increasing U . It is likely that the enhancement in the Rényi entropy is due to antiferromagnetic correlations developed across the two subsystems when the interaction is increased.

In Fig. 7 (a) and (b), S_2^s is rescaled by L^2 and plotted against t_z for $U = 1.0$ and 2.0 respectively. While the data have finite-size fluctuations at small L 's, the figures show reasonably good data collapse, indicating that S_2^s scales as the “volume” of the subsystem, just as in the

free fermion case. In the case of S_2^h , we plot in Fig. 7 (c) and (d) S_2^h/L as a function of inter-layer hopping at $U = 1.0$ and 2.0 . If the system has AF ordering in this parameter range, as demonstrated by the VMC results,³² the entanglement entropy is expected to scale linearly as L . In the region $0 < t_z < 4.0$, the figures seem to suggest that S_2^h scales faster than L . In Fig. 7 (e) and (f), S_2^h/L is fitted to a linear function $\alpha \ln L + \beta$ for several values of t_z . The results for $t_z < 4.0$ suggest that a logarithmic correction to the linear scaling of S_2^h might be possible.

However, in order to differentiate behavior of S_2^h near the phase transition, it is necessary to carry out finite-size scaling study of the Rényi entropy for larger system sizes. In particular, if the logarithmic correction to the linear scaling of S_2^h can be confirmed at $U \lesssim 2.0$, this would indicate possible existence of a Fermi surface. Likewise, a linear scaling of S_2^h is expected in the AF phase when U is sufficiently large compared to the bandwidth. As can be seen from Fig. 6, our data suffers from strong statistical uncertainties in the region of interest. The fluctuations seem to grow with the lattice dimension L and the coupling strength U , making it challenging to simulate large lattices at low temperatures.

We recall that the formalism presented by Eq. (5) requires an explicit computation of the determinant of one-particle Green's functions. At zero temperature, it has been pointed out that the determinant may not exist²⁹ and a thermal broadening scheme is proposed to mend the issue.²⁹ At finite temperatures, it is known⁴⁶ that, even at moderate coupling strengths, the Green's function matrix is ill-conditioned at low temperatures. As an example, the ratio of the largest and smallest eigenvalues of the inverse of the Green's function is of the order 10^{80} on a 16×16 square lattice with $U = 6.0$ and temperature $T/t = 0.067$.⁴⁸ This was the primary issue that plagues large scale DQMC simulations at low temperatures. An efficient matrix decomposition scheme has been proposed to treat the instability issue inherited in DQMC and allows large scale simulations to be carried out successfully.^{48,49} A similar stabilization scheme will

be necessary in order to extract S_2 by directly computing determinants.

Very recently, an alternative method of measuring the entanglement entropies has been proposed.⁴³ The method expresses the Rényi entropy as a logarithmic function of the ratio of two partition functions which can be sampled directly within DQMC scheme. This technique avoids the need of computing determinants and has been shown to be more accurate than Eq. (5).

V. SUMMARY

In this work, we have studied entanglement properties across the AF-BI transition in the bilayer Hubbard model. We focus on two bipartitions illustrated in Fig. 1. Using the correlation matrix method, we have demonstrated that in the tight-binding limit, the second Rényi entropy show sharp signals in the metal-BI transition. For the single-layer partition, the entanglement entropy follows a strict “volume law” due to the singlet formation across the layers. For the two half-layers partition, we were able to show a logarithmic break-down of the “area law” and confirm the prediction based on Widom's conjecture. For the bilayer Hubbard model, we have identified the value of t_z that corresponds to the break-up of singlet pairs across the bilayer, signaling the onset of AF to BI phase transition. However, we were not able to pinpoint the critical point using the entanglement entropy data because of large statistical uncertainties and limited size of simulation cells. Finally, we have commented on the challenges of computing S_2 using the formalism adopted in our study.

ACKNOWLEDGMENTS

CCC and RTS are supported by the DOE grant under the contract number DE-NA0001842-0 and the University of California Office of the President. RRPS acknowledges the support from NSF grant DMR-1306048.

-
- ¹ P. Calabrese and J. Cardy, *J. Stat. Mech.: Theor. Exp.*, **P06002** (2004).
 - ² J. Eisert, M. Cramer, and M. B. Plenio, *Rev. Mod. Phys.* **82**, 277 (2010).
 - ³ M. A. Metlitski, C. A. Fuertes, and S. Sachdev, *Phys. Rev. B* **80**, 115122 (2009).
 - ⁴ M. Levin and X. G. Wen, *Phys. Rev. Lett.* **96**, 110405 (2006).
 - ⁵ A. Kitaev and J. Preskill, *Phys. Rev. Lett.* **96**, 110404.
 - ⁶ S. V. Isakov, R. G. Melko, and M. B. Hastings, *Science* **335**, 193 (2012).
 - ⁷ S. Yan, D. A. Huse, and S. R. White, *Science* **332**, 1173 (2011).

- ⁸ H. C. Jiang, Z. Wang, and L. Balents, *Nature Physics* **8**, 902 (2012).
- ⁹ S. Depenbrock, I. P. McCulloch, and U. Schollwöck, *Phys. Rev. Lett.* **109**, 067201 (2012).
- ¹⁰ J. M. Deutsch, H. Li, and A. Sharma, *Phys. Rev. E* **87**, 042135 (2013).
- ¹¹ L. F. Santos, A. Polkovnikov, and M. Rigol, *Phys. Rev. E* **86**, 010102(R) (2012).
- ¹² M. Storms and R. R. P. Singh, *Phys. Rev. E* **89**, 012125 (2014).
- ¹³ M. M. Wolf, F. Verstraete, M. B. Hastings, and J. I. Cirac, *Phys. Rev. Lett.* **100**, 070502 (2008).
- ¹⁴ S. R. White, *Phys. Rev. Lett.* **69**, 2863 (1992).
- ¹⁵ U. Schollwöck, *Rev. Mod. Phys.* **77**, 259 (2005).

- ¹⁶ J. Jordan, R. Orús, G. Vidal, F. Verstraete, and J. I. Cirac, *Phys. Rev. Lett.* **101**, 250602 (2008).
- ¹⁷ M. B. Hastings, I. González, A. B. Kallin, and R. G. Melko, *Phys. Rev. Lett.* **104**, 157201 (2010).
- ¹⁸ S. Humeniuk and T. Roscilde, *Phys. Rev. B* **86**, 235116 (2012).
- ¹⁹ R. R. P. Singh, M. B. Hastings, A. B. Kallin, and R. G. Melko, *Phys. Rev. Lett.* **106**, 135701 (2011).
- ²⁰ A. B. Kallin, M. B. Hastings, R. G. Melko, and R. R. P. Singh, *Phys. Rev. B* **84**, 165134 (2011).
- ²¹ R. R. P. Singh, R. G. Melko, and J. Oitmaa, *Phys. Rev. B* **86**, 075106 (2012).
- ²² A. B. Kallin, K. Hyatt, R. R. P. Singh, and R. G. Melko, *Phys. Rev. Lett.* **110**, 135702 (2013).
- ²³ A. B. Kallin, E. M. Stoudenmire, P. Fendley, R. R. P. Singh, and G. Melko, Roger, *arXiv:1401.3504*.
- ²⁴ J. Oitmaa, C. Hamer, and W. Zheng, *Series Expansion Methods for strongly interacting lattice models* (Cambridge University Press, 2006).
- ²⁵ V. Eisler and I. Peschel, *J. Stat. Mech. - Theor. and Exp.*, P06005 (2007).
- ²⁶ I. Peschel and V. Eisler, *J. Phys. A - Math. and Theor.* **42**, 504003 (2009).
- ²⁷ H. F. Song, S. Rachel, C. Flindt, I. Klich, N. Laflorencie, and K. Le Hur, *Phys. Rev. B* **85**, 035409 (2012).
- ²⁸ T. Grover, *Phys. Rev. Lett.* **111**, 130402 (2013).
- ²⁹ F. F. Assaad, T. C. Lang, and F. P. Toldin, *arXiv:1311.5851v1*.
- ³⁰ K. Bouadim, G. G. Batrouni, F. Hébert, and R. T. Scalettar, *Phys. Rev. B* **77**, 144527 (2008).
- ³¹ S. S. Kancharla and S. Okamoto, *Phys. Rev. B* **75**, 193103 (2007).
- ³² R. Rüger, L. F. Tocchio, R. Valentí, and C. Gros, *arXiv:1311.6504v2*.
- ³³ L. Wang, K. S. D. Beach, and A. W. Sandvik, *Phys. Rev. B* **73**, 014431 (2006).
- ³⁴ Zheng Weihong, *Phys. Rev. B* **55**, 12267 (1997).
- ³⁵ C. J. Hamer, J. Oitmaa, and Z. Weihong, *Phys. Rev. B* **85**, 014432 (2012).
- ³⁶ D. Gioev and I. Klich, *Phys. Rev. Lett.* **96**, 100503 (2006).
- ³⁷ M. M. Wolf, *Phys. Rev. Lett.* **96**, 010404 (2006).
- ³⁸ W. Li, L. Ding, R. Yu, T. Roscilde, and S. Haas, *Phys. Rev. B* **74**, 073103 (2006).
- ³⁹ B. Swingle, *Phys. Rev. Lett.* **105**, 050502 (2010).
- ⁴⁰ W. Ding, A. Seidel, and K. Yang, *Phys. Rev. X* **2**, 011012 (2012).
- ⁴¹ M. Golor, T. Reckling, L. Classen, M. M. Scherer, and S. Wessel, *arXiv:1409.1103*.
- ⁴² L. Bonnes, H. Pichler, and A. M. Läuchli, *Phys. Rev. B* **88**, 155103 (2013).
- ⁴³ P. Broecker and S. Trebst, *arXiv:1404.3027*.
- ⁴⁴ D. Gioev and I. Klich, *Phys. Rev. Lett.* **96**, 100503 (2006).
- ⁴⁵ H. Widom, *Operator Theory: Adv. Appl.* **4**, 477 (1982).
- ⁴⁶ Z. Bai, W. Chen, R. Scalettar, and I. Yamazaki, in *Multi-Scale Phenomena in Complex Fluids*, edited by T. Y. Hou, C. Liu, and J.-G. Liu (Higher Education Press and World Scientific, Shanghai, China, 2009).
- ⁴⁷ J. Helmes and S. Wessel, *arXiv:1403.7395v1*.
- ⁴⁸ Z. Bai, C.-R. Lee, R.-C. Li, and S. Xu, *Linear Algebra and its Applications* **435**, 659 (2011).
- ⁴⁹ C. N. Varney, C.-R. Lee, Z. J. Bai, S. Chiesa, M. Jarrell, and R. T. Scalettar, *Phys. Rev. B* **80**, 075116 (2009).

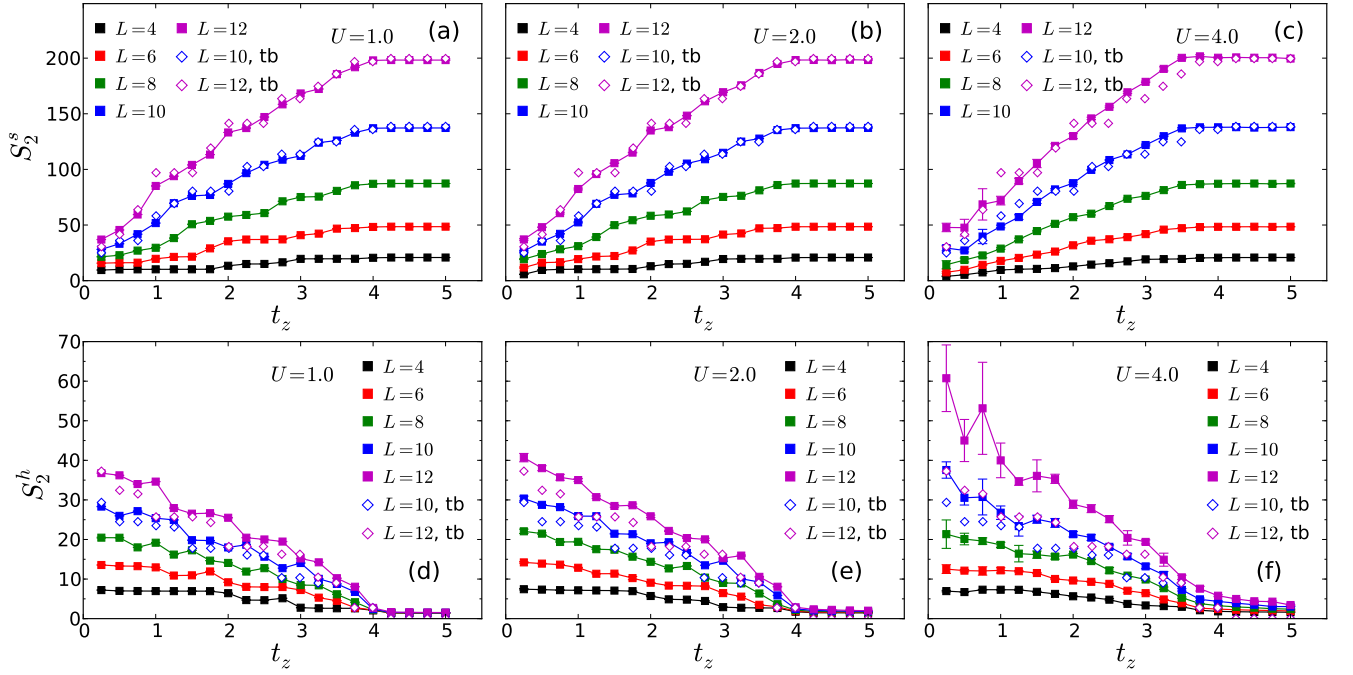


FIG. 6. (Color online) The second Rényi entropy for the bilayer Hubbard model as a function of inter-layer hopping t_z . The upper and lower panels show S_2^s and S_2^h respectively. Simulations are performed at temperature $T/t = 0.05$. Each data point is obtained by averaging over periodic and anti-periodic boundary conditions. In (a)–(c), the empty diamond points represent the ground state S_2^s for the bilayer Hubbard model in the tight-binding (tb) limit $U = 0$ computed using the correlation matrix technique.

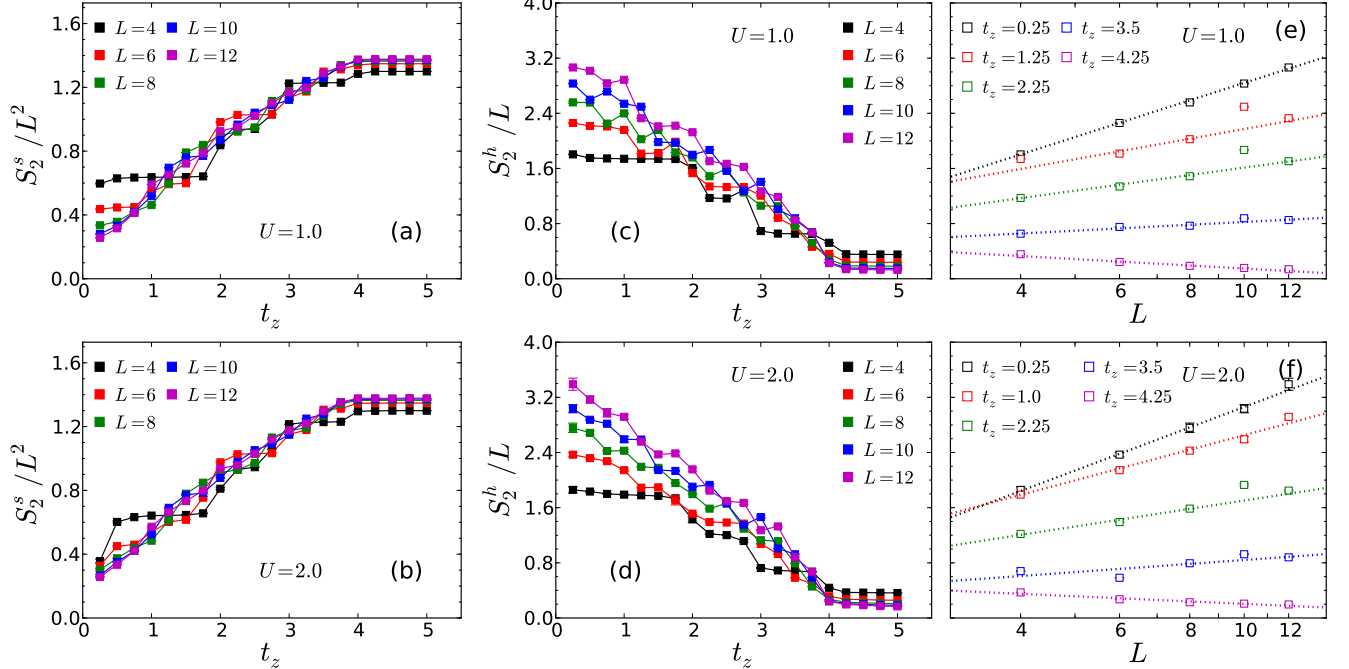


FIG. 7. (Color online) Scaling analysis of the Rényi entropy for the bilayer Hubbard model at $U = 1$ and 2 . Panel (a) and (b): S_2^s/L^2 versus t_z . Both figures show good data collapse, suggesting a “volume law” for S_2^s . Figure (c) and (d): S_2^h/L is plotted against t_z . If the system has an AF order, S_2^h is expected to have a linear scaling in L . The figures, however, do not support the claim for small t_z . In (e) and (f), S_2^h/L is fitted to an ansatz $\alpha \ln L + \beta$. Dotted lines are results of the fit at several representative t_z values. These regression results indicate a possible logarithmic correction to the “area law”.